



# Visible-light-driven *in situ* inactivation of *Microcystis aeruginosa* with the use of floating g-C<sub>3</sub>N<sub>4</sub> heterojunction photocatalyst: Performance, mechanisms and implications



Jingke Song<sup>a,b</sup>, Xuejiang Wang<sup>a,\*</sup>, Jinxing Ma<sup>b,\*</sup>, Xin Wang<sup>a</sup>, Jiayi Wang<sup>a</sup>, Jianfu Zhao<sup>a</sup>

<sup>a</sup> College of Environmental Science and Engineering, State Key Laboratory of Pollution Control and Resource Reuse, Tongji University, Shanghai, 200092, P.R. China; Shanghai Institute of Pollution Control and Ecological Security, Shanghai, 200092, P.R. China

<sup>b</sup> School of Civil and Environmental Engineering, University of New South Wales, Sydney, NSW, 2052, Australia

## ARTICLE INFO

### Keywords:

g-C<sub>3</sub>N<sub>4</sub>  
*Microcystis aeruginosa*  
Visible-light-driven  
Floating photocatalyst

## ABSTRACT

The frequent cyanobacterial harmful algal blooms (cyano-HABs) occurring in aquatic ecosystems pose a threat to human and animal health. In this study, a novel floating, visible-light-driven catalyst was prepared by depositing g-C<sub>3</sub>N<sub>4</sub> on a composite expanded perlite (*i.e.*, EP/Al<sub>2</sub>O<sub>3</sub>) via a facile impregnation-calcination method for the photocatalytic inactivation of *Microcystis aeruginosa*. Consideration has been given to the influence of different dosages of g-C<sub>3</sub>N<sub>4</sub> precursors with the synthesized photocatalysts characterized using XRD, N<sub>2</sub> adsorption/desorption, electron microscopy, FT-IR spectra, XPS and UV-vis absorption spectra. Results of this study show that sheet-like g-C<sub>3</sub>N<sub>4</sub> were well dispersed on the surface of EP/Al<sub>2</sub>O<sub>3</sub> with the heterojunction photocatalyst (CAE-2) with a dicyandiamide to EP/Al<sub>2</sub>O<sub>3</sub> ratio of 2:1 demonstrating the highest specific surface areas (*i.e.*, 56.7 m<sup>2</sup>/g). Under 6 h of irradiation, 74.4% of *M. aeruginosa* at an initial concentration of 2.7 × 10<sup>6</sup> cells/mL could be removed with the use of CAE-2 of 2 g/L. In the photocatalytic inactivation process, algae cell lysis is mainly ascribed to the attack by the reactive oxygen species (ROSs) generated on the semiconductor surface, with the predominant species (*i.e.*, HO·) causing the damage of membrane permeability with cations and cellular organic matters released into the solution though the cellular organic matters including microcystin-LR could readily be removed by the photocatalysts. Continuous monitoring by using flow cytometry and measuring the maximum photochemical efficiency of PSII indicated that cell apoptosis and reduction of photosynthetic activity occurred as a result of the inactivation. This study presents a promising technology for the remediation of cyano-HABs in open waters.

## 1. Introduction

The occurrence of frequent harmful algal blooms of cyanobacteria (cyano-HABs) in eutrophic water bodies pose a threat to users with the toxic metabolites released (such as microcystin-LR from *Microcystis aeruginosa*) exhibiting acute poisoning and chronic cancer promotion potential [1–3]. It is alleged that climate change has amplified the severity of this problem; for instance, using high-resolution sea-surface temperature records to model trends in growth rates and bloom-season duration for *Alexandrium fundyense* and *Dinophysis acuminata*, Gobler et al. [4] concluded that ocean warming since 1982 has significantly expanded the niche of cyano-HABs in the North Atlantic and North Pacific oceans.

To date, a number of control and/or remediation tactics including mechanical separation, chemical adsorption and biological degradation

in response to the increasing occurrence of cyano-HABs have been developed [5] with technologies based on photocatalysis gaining in popularity because of their high efficiency, environmental sustainability and low cost of operation [6–8]. For example, Pinho et al. [9] investigated the destruction of the cyanobacteria, *M. aeruginosa*, with simultaneous removal of microcystin-LR with a solar driven titanium dioxide (TiO<sub>2</sub>) photocatalytic process, and Natarajan et al. [10] developed Ag and TiO<sub>2</sub> nanoparticle (NP)-incorporated nanocomposite against freshwater algae. While near UV active TiO<sub>2</sub> photocatalysts are gaining popularity in water/wastewater purification and disinfection [7,11], materials such as anatase are of less interest given that they can only be activated by light with wavelengths below 380 nm [12,13]. In addition to tailoring of the traditional TiO<sub>2</sub> through element doping and/or surface grafting (*e.g.*, N-TiO<sub>2</sub>) making visible-light-driven (VLD) photocatalysis a possibility [1,14], recent evidence demonstrates that a

\* Corresponding authors.

E-mail addresses: wangxj@tongji.edu.cn, 2015wxj@tongji.edu.cn (X. Wang), jinxing.ma@unsw.edu.au (J. Ma).

group of VLD semiconductors including graphitic carbon nitride ( $\text{g-C}_3\text{N}_4$ ) and its hybrids can be successfully prepared from simple precursors at low cost [7,9,13,15]. It has been reported that the relatively narrow band gap of  $\text{g-C}_3\text{N}_4$  (2.70 eV) as a result of the tri-s-triazine units connected with planar amino groups results in high VLD activity whilst the delocalized conjugated  $\pi$  structures lead to rapid photo-induced charge separation, with the recombination of electron-hole pairs further retarded via coupling with other semiconductors [16,17].

Given the advantages of  $\text{g-C}_3\text{N}_4$ , numerous studies have been conducted involving the use of this material in energy production and organic pollutant degradation [18–20]. While several more recent attempts have been carried out addressing the disinfection applications including inactivation of MS2 by metal-free  $\text{g-C}_3\text{N}_4$  [7], and *E. coli* using  $\text{g-C}_3\text{N}_4/\text{TiO}_2$  [13] and/or graphene/ $\text{g-C}_3\text{N}_4$  nanosheets cowrapped elemental  $\alpha$ -sulfur [15], there is, to the best of our knowledge, no report on the control of cyano-HABs using this novel photocatalyst group. One expected technology challenge in the application of  $\text{g-C}_3\text{N}_4$  in natural systems is that photosynthetic cyanobacteria are apt to grow on the water surface where sunlight is available [21,22], while nano-size  $\text{g-C}_3\text{N}_4$  are inclined to aggregate (and settle down) in non-stirred reservoirs, therefore hindering the contact between algae and photocatalysts [23]. Moreover, the separation and recycling of nano-size  $\text{g-C}_3\text{N}_4$  are difficult and their residual and migration in the environment might arouse serious health concerns [24]. To solve these problems, there is a possibility to develop floating photocatalysts based on different floating substrates such as expanded graphite [25], expanded perlite [8,23], fly ash cenospheres [26] and low density polyethylene [27]. It is expected that these composite photocatalysts are especially suitable for solar-driven remediation of non-stirred and non-oxygenated reservoirs [27].

In the present work, we first synthesized a novel floating  $\text{g-C}_3\text{N}_4$  heterojunction photocatalyst via a facile impregnation-calcination method with expanded perlite (EP) loaded with amorphous  $\text{Al}_2\text{O}_3$  as a porous floating carrier. The use of amorphous  $\text{Al}_2\text{O}_3$  could increase the active sites of carriers whilst, possibly, transferring photo-induced electrons of  $\text{g-C}_3\text{N}_4$  [28]. We have found the samples synthesized showed a good contact with algae near the water surface and could readily be withdrawn following remediation. Consideration was therefore given to the impacts of different dosages of  $\text{g-C}_3\text{N}_4$  precursors on the performance of the photocatalysts with *M. aeruginosa* chosen as a model strain in evaluation of the photocatalytic inactivation activity. The overarching goal of this study is to provide an effective, low-cost technology to control cyano-HABs in natural water bodies and to elucidate the scenario likely prevailing in the photocatalytic inactivation process.

## 2. Materials and methods

### 2.1. Materials and reagents

The expanded perlite (EP) was obtained from Xinyang Zhongke Mining Industry Co. Ltd. (Henan, China) and their particle sizes were 1–3 mm.

All chemicals were purchased from Sinopharm Chemical Reagent Beijing Co., Ltd. (China) unless otherwise mentioned, and they were of reagent grade or higher purity and used without further purification. Aqueous solutions utilized were prepared with deionized water. *M. aeruginosa* cells (strain number: FACHB-913) were purchased from Freshwater Algae Culture Collection at the Institute of Hydrobiology in Wuhan (China). The algae were cultivated at 25 °C in 1 L of sterilized BG-11 medium (Ingredients of the medium could be found in Section S1 in Supporting Information) at low-speed shaking. Illumination intensity for incubation was ~2000 Lux with a light/dark cycle of 12 h/12 h.

### 2.2. Preparation of the floating $\text{g-C}_3\text{N}_4$ heterojunction photocatalyst

$\text{EP}/\text{Al}_2\text{O}_3$  carriers were prepared according to the protocols with minor modification [28,29]. Briefly, 1.5 g  $\text{Al}(\text{NO}_3)_3 \cdot 9\text{H}_2\text{O}$  and 1.2 g urea was dissolved in 10 mL deionized water followed by the addition of 1 g EP. The flask was shaken on a thermostat shaker at 120 rpm at room temperature for 1 h, and then dried in an oven at 80 °C for 12 h. Subsequently, the resultant slurry was heated in a muffle furnace under atmosphere at 300 °C for 2 h. In this study, the acronym  $\text{EP}/\text{Al}_2\text{O}_3$  is used for EP floating carriers loaded with  $\text{Al}_2\text{O}_3$ .

In order to seed  $\text{g-C}_3\text{N}_4$  on the surface of  $\text{EP}/\text{Al}_2\text{O}_3$ , a facile impregnation-calcination method was introduced; typically, a certain amount (0.5, 1, 2 or 3 g) of  $\text{g-C}_3\text{N}_4$  precursors, dicyandiamide [30], was dissolved in 20 mL deionized water, and then 2 g  $\text{EP}/\text{Al}_2\text{O}_3$  was added into the solution under ultrasonic for 1 h followed by heated at 80 °C to remove water. The resultant mixture was then heated to 550 °C for 2 h with a heating rate of 10 °C/min in a muffle furnace with a covered alumina crucible. During the heat and calcination processes, the dicyandiamide was expected to attach onto the surface of  $\text{EP}/\text{Al}_2\text{O}_3$  with  $\text{g-C}_3\text{N}_4$  generated. After cooling down to ambient temperature, the  $\text{g-C}_3\text{N}_4$  composites were then loaded on an open alumina crucible and annealed in a muffle furnace at 500 °C for 2 h to produce exfoliated  $\text{g-C}_3\text{N}_4$  on the surface [31]. The photocatalysts were termed CAE-x with x representing the different dosages of dicyandiamide (i.e., 0.5, 1, 2 or 3 g). For comparison,  $\text{g-C}_3\text{N}_4$  was prepared with the same heating and exfoliating protocol without the addition of  $\text{EP}/\text{Al}_2\text{O}_3$ . To determine the role of  $\text{Al}_2\text{O}_3$  layer, photocatalyst CE-2, i.e., CAE-2 without the use of  $\text{Al}_2\text{O}_3$  was also prepared with the same protocol of CAE-2.

### 2.3. Photocatalytic inactivation of *M. aeruginosa*

Photocatalytic activities of the  $\text{g-C}_3\text{N}_4$  composites in inactivation of *M. aeruginosa* were evaluated in a DY-F photochemical reactor (Shanghai Deyangyibang Instruments Co., Ltd. China). A 500 W Xe lamp (XE-JY500) equipped with a UV filter at a distance of 10 cm from the beaker was used as the light source, with the luminous intensity maintained at ca. 2 mW/cm<sup>2</sup> for all experiments. There was a cooling system to eliminate the thermal effects. *M. aeruginosa* at the exponential growth phase were withdrawn from the incubation medium by centrifugation at 8000 rpm for 5 min and diluted with deionized water with the pH controlled at 7.2. Because the maximum absorbance band of *M. aeruginosa* suspensions appears around 680 nm in the UV-vis spectrum, in this study, the initial cell concentrations of algae solutions were measured on a Shimadzu UV-2700 spectrophotometer at the wavelength of 680 nm [32]. The initial concentrations of algae were about  $2.7 \times 10^6$  cells/mL, corresponding to an  $\text{OD}_{680}$  of 0.2. In all experiments, 0.1 g photocatalyst and 50 mL of algae solution were added into one quartz glass tube set of the reactor. Low-speed magnetic agitation was used to simulate the flow turbulence in natural water bodies [23]. Prior to illumination, the mixtures were subject to dark treatment to reach adsorption equilibrium according to our preliminary studies. The photocatalytic inactivation experiments were then performed for 6 h under visible light irradiation. At pre-determined intervals, 500  $\mu\text{L}$  of the suspension were collected and analyzed to obtain the counting cell concentrations using a hemacytometer (Brand GmbH, Wertheim, Germany) in combination with a phase contrast microscope (ML32 Microshot Technology, Guangzhou, China).

### 2.4. Analytical methods

In this study, X-ray diffraction (XRD), Brunauer-Emmett-Teller (BET) surface analysis, field-emission scanning electron microscopy (FESEM) with energy dispersive spectrometry (EDS), transmission electron microscopy (TEM), Zeta potential, Fourier transform infrared spectrometry (FTIR), and X-ray photoelectron spectrometry (XPS) and UV-vis absorption spectra were used to characterize the catalyst

properties with details about the methodologies provide in Section S2.

Morphology changes of the algal cells in the solution were analyzed with the use of a Nikon Eclipse 80i fluorescence microscope equipped with a digital camera (DS-Ri1, Nikon). Alexa Fluor 488 annexin V/Dead Cell Apoptosis Kits (catalog no. V13241, 488 annexin V ex/em: 488/499 nm; Propidium iodide ex/em: 535/617 nm) purchased from Invitrogen Life Technologies (Carlsbad, CA) were used to investigate the algal cell viability. The algae suspensions following staining according to the manufacturer protocol were examined in a Gallios Flow Cytometer (Beckman Coulter, Brea, CA) at 530 nm (i.e., FL1) and >575 nm (i.e., FL3) with the data analyzed using Gallios software. Photosynthetic activities of the algae were determined with a PHYTO-PAM phytoplankton analyzer (Heinz Walz, German). The samples were dark-adapted for 30 min prior to the determination of the minimal ( $F_0$ ) and maximal ( $F_m$ ) fluorescence yields, corresponding to the open and closed PSII reaction centers respectively [32]. The maximum quantum yield of PSII ( $F_v/F_m$ ) was calculated as  $(F_m - F_0)/F_m$  [33]. Ion concentrations were measured using an Inductive Coupled Plasma Emission Spectrometer (ICP-OES) (Agilent 720ES). Three-dimensional excitation and emission matrix (EEM) fluorescence spectroscopy of the cellular organic matters (COM) was analyzed using a HORIBA FL-4 max spectrometer [34].

Determination of microcystin-LR was carried out on a Shimadzu LC-20A system with a PDA detector and a C<sub>18</sub> reverse-phase column (250 mm × 4.6 mm × 5 μm, Agilent). The mobile phase was water containing 0.05% TFA (v/v) and methanol with the ratio of 35:65. The injection volume of the samples was 20 μL and the flow rate was 0.6 mL/min. The wavelength of the UV absorbance detector was 238 nm [35].

### 3. Results and discussion

#### 3.1. Characterization of the floating g-C<sub>3</sub>N<sub>4</sub> heterojunction photocatalysts

The phase structure and crystallinity of the prepared catalysts were investigated by XRD. As shown in Fig. 1a, following the deposition of Al<sub>2</sub>O<sub>3</sub> on the surface of EP, peaks at 22.6°, 28.8°, 33.0° and 39.5° were observed in EP/Al<sub>2</sub>O<sub>3</sub>. It is allegedly the peak at 39.5° is assigned to the diffraction of (222) of γ-Al<sub>2</sub>O<sub>3</sub> [36] with the peak at 22.6° attributed to the heterojunction of SiO<sub>2</sub>/Al<sub>2</sub>O<sub>3</sub> [37] though other peaks are largely different from that of the pure Al<sub>2</sub>O<sub>3</sub> sample (Fig. 1a). A plausible explanation is that Al<sub>2</sub>O<sub>3</sub> in EP/Al<sub>2</sub>O<sub>3</sub> is of low abundance with the dispersion homogeneous. Two pronounced peaks were found in the pure g-C<sub>3</sub>N<sub>4</sub> sample at 27.4° and 13.1°, corresponding to the long-range interplanar stacking of the conjugated aromatic system and the interlayer structural packing respectively [38]. With regard to the CAE hybrids, when the dosage of dicyandiamide was lower than 3 g/2 g-EP/Al<sub>2</sub>O<sub>3</sub>, g-C<sub>3</sub>N<sub>4</sub> was not detected (Fig. 1a). This finding is, however, not surprising because previous studies have indicated that g-C<sub>3</sub>N<sub>4</sub> is a low crystalline organic matter and its peaks could easily be depressed by the high crystalline materials from the matrix [38,39]. In comparison, a small characteristic peak relating to g-C<sub>3</sub>N<sub>4</sub> at 2θ of 27.4° has been observed in CAE-3, and it was indexed as (002) reflections in good agreement with JCPDS 87–1526 [28]. No predominant peaks of Al<sub>2</sub>O<sub>3</sub> were found in the g-C<sub>3</sub>N<sub>4</sub> heterojunction photocatalysts, likely ascribed to the cover of g-C<sub>3</sub>N<sub>4</sub> that resulted in the signal of Al<sub>2</sub>O<sub>3</sub> disappearing.

The N<sub>2</sub> adsorption-desorption isotherms of different samples are shown in Fig. 1b with the BET specific surface areas and pore volumes provided in Table S1. Specifically, with the modification of Al<sub>2</sub>O<sub>3</sub>, the specific surface areas of EP significantly increased from 2.3 m<sup>2</sup>/g to 31.6 m<sup>2</sup>/g, and the N<sub>2</sub> adsorption-desorption isotherm of EP/Al<sub>2</sub>O<sub>3</sub> presented the pattern of type (III) according to IUPAC stands, indicating the presence of macroporous pores in the material [40]. Following the deposition of g-C<sub>3</sub>N<sub>4</sub> on the surface of EP/Al<sub>2</sub>O<sub>3</sub>, the formation of g-C<sub>3</sub>N<sub>4</sub> nanoparticles inside the porous structure led to a further increase in the specific surface area of catalysts (Fig. 1b and Table S1). Notably,

CAE-2 showed the highest specific surface area (i.e., 56.7 m<sup>2</sup>/g) and the highest porosity while the smallest average pore size among the CAE-x samples (Table S1). In this study, all CAE-x isotherms demonstrated a hysteresis of H3 type (Fig. 1b), which should be attributed to slited-shaped pores formed from the aggregates of plate-like particles [41], suggesting the presence of g-C<sub>3</sub>N<sub>4</sub> nanosheets on the surface of heterojunction photocatalysts.

The surface morphological properties of the CAE-2 were analyzed using FESEM with the distribution of different elements determined by EDS. Fig. S1 depicts the FESEM images of EP and EP/Al<sub>2</sub>O<sub>3</sub>, and it can be hypothesized the formation of rod-/needle-like amorphous Al<sub>2</sub>O<sub>3</sub> on the material surface should account for the increase in the specific surface area of EP/Al<sub>2</sub>O<sub>3</sub> (Table S1). With the deposition of g-C<sub>3</sub>N<sub>4</sub>, sheet-like structures were found on the surface of the catalyst (Fig. 1c). As shown in Fig. S2, signals from C, N, O, Na, Al, Si, K and Fe were detected using EDS with mapping of the concerned elements including Al, C and N suggesting a well dispersion of Al<sub>2</sub>O<sub>3</sub> and g-C<sub>3</sub>N<sub>4</sub> on the surface of the heterojunction photocatalyst (Figs. 1d-f). Moreover, TEM micrographs of EP/Al<sub>2</sub>O<sub>3</sub> and CAE-2 (Fig. S3) demonstrated that the loose-packed Al<sub>2</sub>O<sub>3</sub> covered on EP likely provided a great number of active sites for the deposition of g-C<sub>3</sub>N<sub>4</sub> with g-C<sub>3</sub>N<sub>4</sub> on the surface of CAE-2 displaying two dimensional and overlapped lamellar structures. Furthermore, the zeta potentials of EP, AE, g-C<sub>3</sub>N<sub>4</sub> and CAE-2 were −36.9, 41.1, −26.8 and −5.57 mV, respectively, which also indicated that Al<sub>2</sub>O<sub>3</sub> and g-C<sub>3</sub>N<sub>4</sub> were successful modified on the surface of EP in CAE-2.

To further elucidate the interaction of g-C<sub>3</sub>N<sub>4</sub> with the catalyst surface, FTIR was firstly performed. It could be observed from Fig. 2a that the band of 1385 cm<sup>−1</sup> attributed to the vibration of NO<sub>3</sub><sup>−</sup> groups from the residual of Al(NO<sub>3</sub>)<sub>3</sub> [28] is only noted in the EP/Al<sub>2</sub>O<sub>3</sub> spectrum. In comparison, the FTIR spectra of CAE-2 and pure g-C<sub>3</sub>N<sub>4</sub> showed similar patterns; there were three characteristic bands including the peak at 809 cm<sup>−1</sup> related to out-of plane bending modes of C–N heterocycles, the band in the range of 1319–1557 cm<sup>−1</sup> to the typical stretching vibration of C–N heterocycles and the absorption band at 1638 cm<sup>−1</sup> to the C–N stretching vibration [42,43]. All these observations exemplified the successful loading of g-C<sub>3</sub>N<sub>4</sub> on the surface of EP/Al<sub>2</sub>O<sub>3</sub>. Fig. S4 depicts the XPS survey spectrum of CAE-2 containing four elements of Al, C, N and O. Specially, the intensity of N peak was low with a plausible explanation that the thermal oxidation etching promoting the formation of thin g-C<sub>3</sub>N<sub>4</sub> nanosheets led to the loss of C and N atoms [44]. Fig. 2b shows the high-resolution C 1s spectrum with three principal components found at 285.9, 287.2 and 289.6 eV after deconvolution. The peak with lower bonding energy (285.9 eV) should be associated with the sp<sup>2</sup>-hybridized C atoms bonded to N inside the aromatic structures [45]. The second component shifting towards higher energy value at 287.2 eV stems from sp<sup>2</sup>-hybridized C in the aromatic ring attached to an electronegative group [45]. The third C 1s peak at 289.6 eV is allegedly ascribed to the presence of carboxylate carbon (O=C=O) [46]. Meanwhile, the high-resolution N 1s spectrum of CAE-2 revealed three peaks located at 398.4, 399.8 and 401.4 eV (Fig. 2c), which can respectively be indexed to C–N–C, N-sp<sup>3</sup>C and N–H groups [44,47]. As for the Al 2p XPS spectrum shown in Fig. 2d, two peaks at binding energy of 75.0 and 76.2 eV have been observed. While the component at 76.2 eV represents the oxide and/or hydroxide structures bonded to aluminum [48], the other at 75.0 eV could be considered as an indicator of interaction between Al and N because a red shift of ~0.6 eV from 74.4 eV of a typical Al–N bond is likely expected with an increase in the effective negative charge on Al species as a result of the presence of surface hydroxyl groups from g-C<sub>3</sub>N<sub>4</sub> (Fig. 2b) [28,48].

Fig. S5 provides the UV-vis absorption spectra of g-C<sub>3</sub>N<sub>4</sub>, EP, EP/Al<sub>2</sub>O<sub>3</sub> and CAE-2. While it could be observed that both EP and EP/Al<sub>2</sub>O<sub>3</sub> demonstrated negligible visible light absorption, the heterojunction photocatalyst following the introduction of g-C<sub>3</sub>N<sub>4</sub> exhibited considerable light absorption ability in the visible light region. Moreover, the

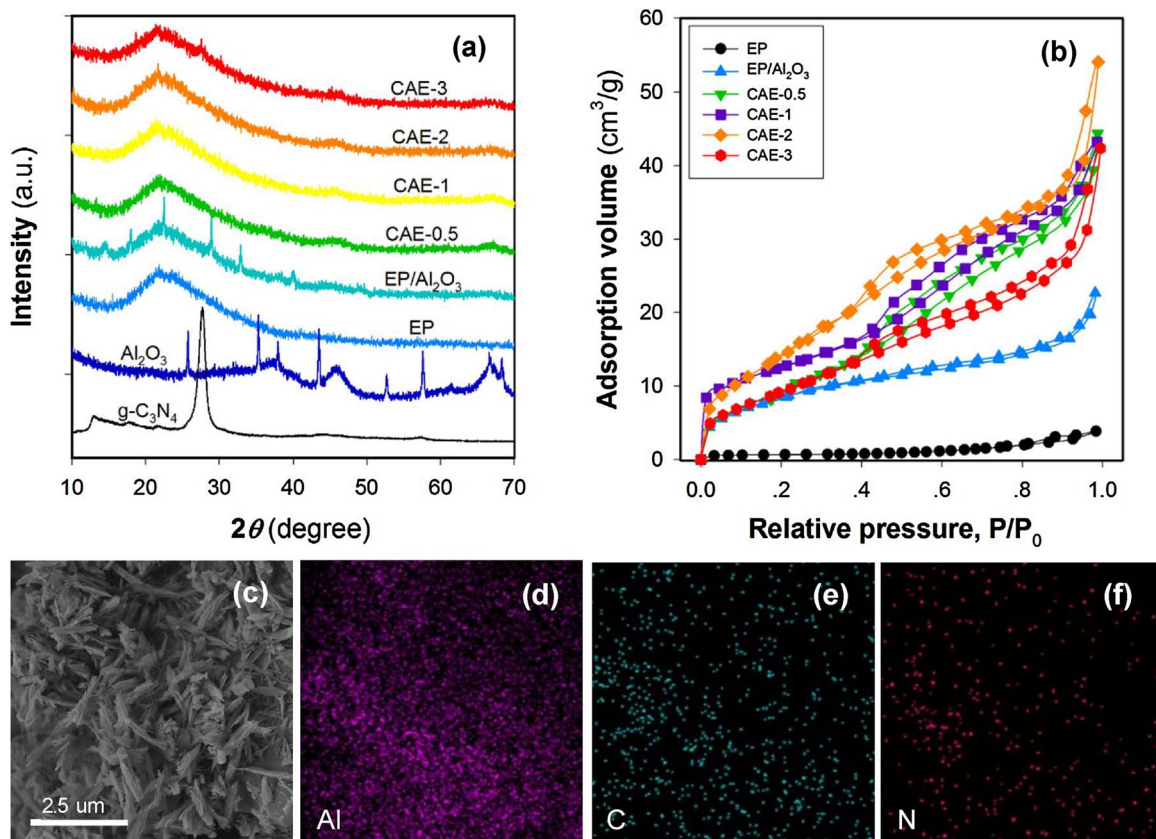


**Fig. 1.** Characterization of the floating  $\text{g-C}_3\text{N}_4$  heterojunction photocatalysts. (a) XRD patterns of pure  $\text{g-C}_3\text{N}_4$ ,  $\text{Al}_2\text{O}_3$ , EP,  $\text{EP}/\text{Al}_2\text{O}_3$  and various hybrid samples, (b)  $\text{N}_2$  sorption isotherms of EP,  $\text{EP}/\text{Al}_2\text{O}_3$  and CAE- $x$  ( $x = 0.5, 1, 2$  or  $3$ ) and (c) FESEM image of CAE-2 with element mapping images of Al, C and N provided in (d), (e) and (f) respectively.

light absorption threshold of CAE-2 did not show much difference compared to the pure  $\text{g-C}_3\text{N}_4$ , though the absorption strength decreased because of the low amount of  $\text{g-C}_3\text{N}_4$  loaded on the surface.

### 3.2. Photocatalytic inactivation of *M. aeruginosa*

Fig. 3a shows the results of photocatalytic inactivation of *M. aeruginosa* suspensions using CAE with different  $\text{g-C}_3\text{N}_4$  loadings. The changes of cell density with no addition of photocatalyst (*i.e.*, control test) and with the use of EP or  $\text{EP}/\text{Al}_2\text{O}_3$  were also investigated for comparison. As can be seen from Fig. 3a, the cell density in the solution slightly decreased in the absence of photocatalysts, which indicated the light solely contributed insignificantly to the algal destruction [23]. When the pristine EP or  $\text{EP}/\text{Al}_2\text{O}_3$  was used, the removal rates of *M. aeruginosa* reached 17.3–24.1% following a rapid adsorption process in darkness (0.5 h) though a slow decrease in cell density was observed under irradiation. In comparison (Fig. 3a), photocatalytic inactivation of *M. aeruginosa* was significantly enhanced with the induction of  $\text{g-C}_3\text{N}_4$ . Overall, CAE-2 demonstrated the highest performance among the catalysts; *i.e.*, 43.7% of *M. aeruginosa* were removed from the aqueous solution as a result of dark adsorption, with the inactivation efficiency increased to 74.7% following 6 h of VLD photocatalysis. Therefore, subsequent experiments were carried out using CAE-2 unless otherwise stated.

It was initially hypothesized that the outstanding performance of  $\text{g-C}_3\text{N}_4$  heterojunction photocatalysts should be ascribed to the synergistic effect of photocatalytic activity and adsorption capacity, resulting in a critical concern that the efficiency would be declined as a result of the exhaustion of adsorption active sites. As can be seen from Fig. 3b, following three successive cycles, the adsorption capacity of CAE-2 was substantially decreased and became quite similar to that of EP or  $\text{EP}/\text{Al}_2\text{O}_3$  (Fig. 3a). In contrast, the removal rates of *M. aeruginosa*

following 6 h of photocatalysis sustained (Fig. 3b). These findings suggested that the oxidation process using  $\text{g-C}_3\text{N}_4$  heterojunction photocatalysts was efficacious to degrade most of the algae adsorbed on the catalyst surface though the deposition of algal inorganic debris (Fig. S6) likely led to the loss of adsorption capacity.

Validation of the removal of *M. aeruginosa* via photocatalysis rather than adsorption was conducted by measuring the fluorescence parameter  $F_v/F_m$ , which is an indicator of the maximum photochemical efficiency of PSII (maximal PSII quantum yield) [32].  $F_v/F_m$  reflects the effects of environmental stress factors on the phytoplankton growth [49]. As shown in Fig. 3c, the adsorption with the use of  $\text{EP}/\text{Al}_2\text{O}_3$  over 6.5 h did not cause significant decline in  $F_v/F_m$ . In contrast, although the exposure of algal cells to CAE-2 in the dark condition did not result in obvious inhibition on the photosynthetic activity,  $F_v/F_m$  was substantially decreased in the subsequent photocatalysis process (Fig. 3c). Notably, the photosynthetic activity of *M. aeruginosa* dropped to a very low level of 0.12 at the end of the experiment, which is much lower than the values (0.40–0.47) indicating the good growth of *Microcystis* in aqueous environments [49,50].

With regard to the adverse impacts of algae degradation on adsorption, consideration was given to the interference of natural organic matters on the photocatalytic inactivation of *M. aeruginosa* under visible-light irradiation. Different concentrations (1, 2, 4 and 6 mg/L) of humic acids (HA) were added into the algal solution [51]. As shown in Fig. S7, the addition of HA obviously inhibits the adsorption of algal cells in the dark environment, while the photocatalytic inactivation of *M. aeruginosa* was enhanced at low concentration of HA ( $\leq 2$  mg/L) which might be related to the photosensitization of HA. In contrast, slight suppression was noted at high HA concentration ( $\geq 4$  mg/L) due to its competitive adsorption of photons and/or reactive oxygen species (ROSs) with algal cells [52]. Overall, the presence of natural organic matters did not lead to significant deterioration of the photocatalytic

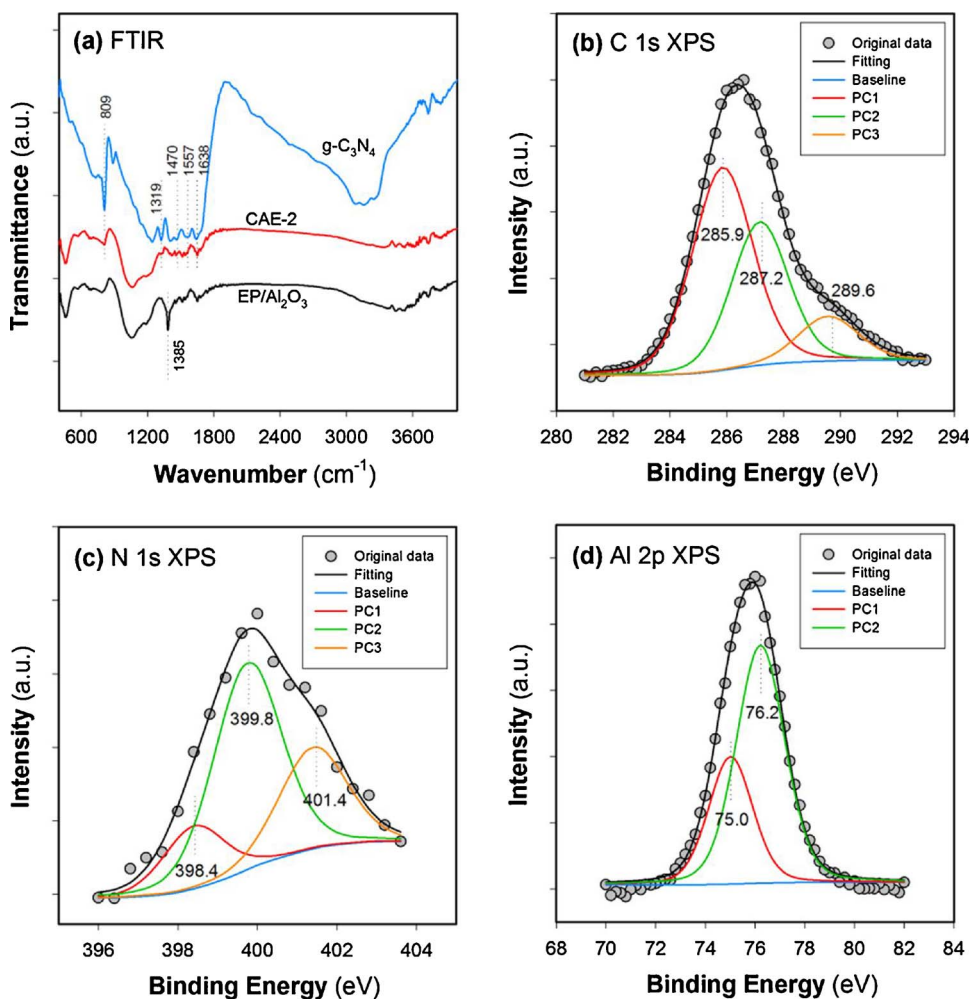


**Fig. 2.** Surface modification of g-C<sub>3</sub>N<sub>4</sub> on heterojunction photocatalysts. (a) FTIR spectra of g-C<sub>3</sub>N<sub>4</sub>, EP/Al<sub>2</sub>O<sub>3</sub> and CAE-2 and high-resolution XPS spectra of (b) C 1s, (c) N 1s and (d) Al 2p of CAE-2. In Fig. 2b-d, PC indicates the principle component after deconvolution.

inactivation.

### 3.3. Deconstruction of *M. aeruginosa* and its impacts on the environment

To elucidate the effects of photocatalysis on *M. aeruginosa*, the optical microscopy was introduced to observe the changes in the cell morphology. Fig. 4a and b show the images of initial algae cells and

that following 0.5 h of dark adsorption with the use of CAE-2. It can be noted that most *M. aeruginosa* demonstrated intact cytoderm and epicyte after the adsorption treatment. With the exposure to irradiation, the cell density rapidly decreased with some algae no longer being spherical (Figs. Fig. 3a and Fig. 4c). Following 6 h of treatment, ruptures were observed on the surface of most cells (Fig. 4d). Quantification of the algae viability was then carried out using the flow cytometry

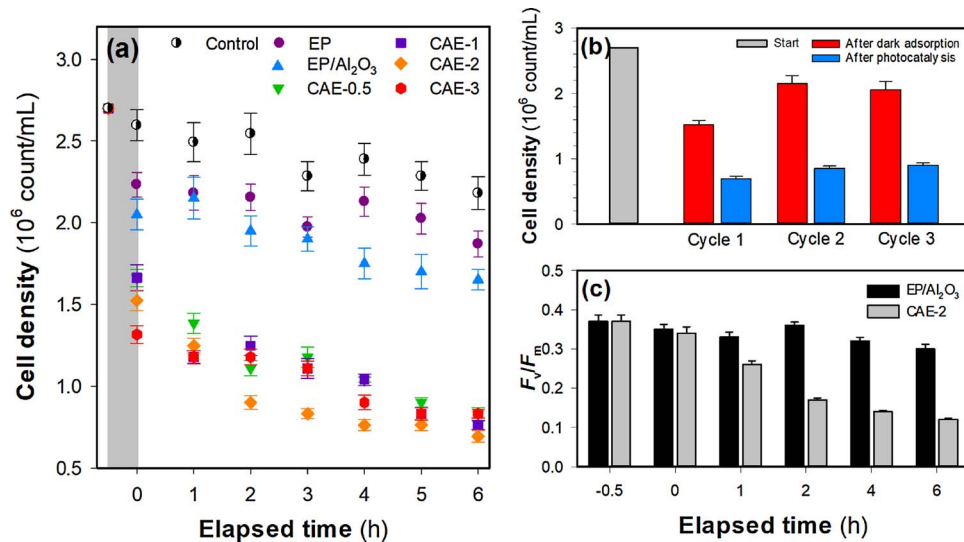


**Fig. 3.** Photocatalytic inactivation of *M. aeruginosa*. (a) Comparison of the efficiency with no addition of photocatalyst, and the use of EP, EP/Al<sub>2</sub>O<sub>3</sub> or g-C<sub>3</sub>N<sub>4</sub> photocatalysts (CAE-x), (b) Changes in the efficiency of CAE-2 for the adsorption (i.e., after dark adsorption) and the degradation (i.e., after 6 h of photocatalysis) in three successive cycles, and (c) Changes in the photosynthetic activity of *M. aeruginosa* with the use of EP/Al<sub>2</sub>O<sub>3</sub> and CAE-2. Experiment conditions: catalyst = 0.1 g, reaction volume = 50 mL, initial cell density =  $2.7 \times 10^6$  cells/L and pH = 7.2. In Fig. 3a and c, the shade area and/or the period from  $-0.5$  to 0 h indicate the dark adsorption stage.

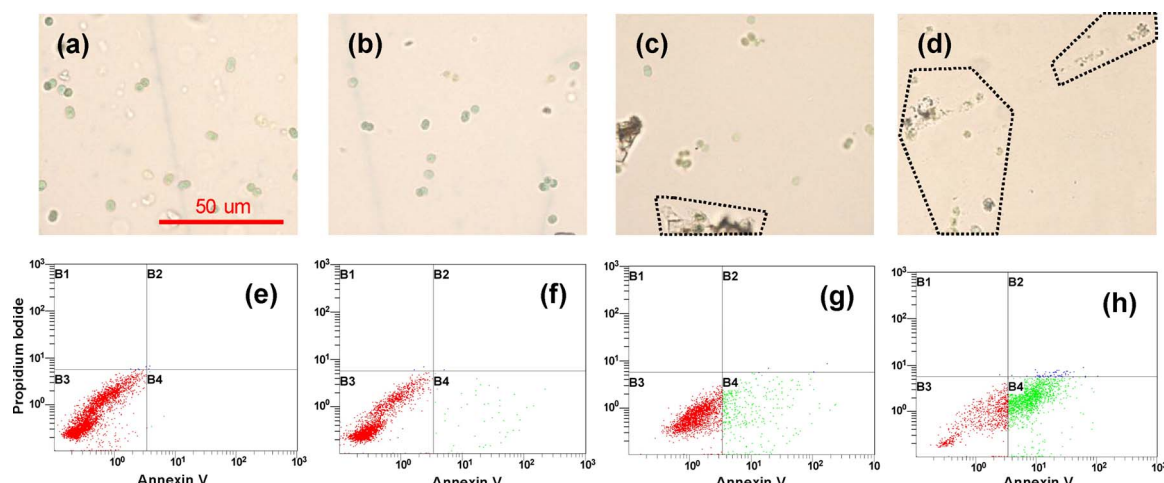


**Fig. 4.** Microscope images of (a) initial algal cells and that following (b) 0.5 h adsorption in dark, (c) 2 h and (d) 6 h of photocatalytic inactivation, and flow cytometry analysis with Annexin V and Propidium Iodide (PI) staining: Annexin V vs. PI plots of (e) initial algal cells and that following (f) 0.5 h of adsorption in dark, (g) 2 h and (f) 6 h of photocatalytic inactivation. Experiment conditions: CAE-2 = 0.1 g, reaction volume = 50 mL, initial cell density =  $2.7 \times 10^6$  cells/L and pH = 7.2. Polygons in Fig. 4c and d indicate the damaged cells. In Fig. 4e–h, B1: Annexin<sup>−</sup>PI<sup>+</sup> (non-viable cells: necrotic cells); B2: Annexin<sup>+</sup>PI<sup>+</sup> (non-viable cells: late apoptotic cells); B3: Annexin V<sup>−</sup>PI<sup>−</sup> (viable cells); B4: Annexin<sup>+</sup>PI<sup>−</sup> (non-viable cells: early apoptotic cells).

combined with fluorescent staining. In accordance with the results of photosynthetic activity (Fig. 3c), the dark incubation of *M. aeruginosa* in the solution containing CAE-2 did not lead to significant cell damage as B3 zones indicating the living cells in Fig. 4e and f account for 99.6% and 97.7% of the total counts respectively. However, after 2 h of irradiation, a small group of the algae (i.e., B4 zone including 14.6% of cell counts in Fig. 4g) were assigned into early apoptotic cells with a loss of the metabolic activity. With the photocatalysis extended to 6 h, the portion of B4 zone had increased to 65.4%, and 2.02% of the total counts were assigned into B2 zone that indicates the severe damage of the membrane (i.e., late apoptotic cells) [53].

While destruction of *M. aeruginosa* with the use of g-C<sub>3</sub>N<sub>4</sub> heterojunction photocatalysts under irradiation has been emphasized above, there is a critical concern aroused relating to the release of cellular matters including Microcystin-LR (MC-LR) that might result in health risks. Fig. S8 show the exposure to photocatalytic treatment had affected the cell membrane permeability and/or disturbed the metabolic pathways of *M. aeruginosa* because of a rapid increase in K<sup>+</sup>, Na<sup>+</sup> and Ca<sup>2+</sup> concentrations in the aqueous solution exemplifying that the algae were incapable of selectively transferring extracellular K<sup>+</sup> and Ca<sup>2+</sup> into cells [54]. In addition, there was no Al<sup>3+</sup> detected during the reaction, which indicated the fabricated materials were of relatively high stability. The concomitant release of cellular organic matters (COM) into the aqueous solution during photocatalysis was then analyzed using the three-dimensional EEM fluorescence spectroscopy. It can be observed from Fig. 5a that the EEM fluorescence spectrum of the initial algae solution contains peak A at ex/em of 280/330 representing the occurrence of protein-like substances [34,55,56], likely ascribed to the extracellular organic matter (EOM) secreted by *M. aeruginosa*. Following 2 h of photocatalytic treatment, there are another two peaks observed in the EEM spectrum (Fig. 5b) with peaks B and C reported to be indicators of humic-like substances in solutions [55,57]. An increase in the intensity of peak A could be regarded as the release of COM and/or dissociation of EOM while the humic-like substances might originate from the residual organic matters as a result of the decomposition of algal cells and/or COM and EOM during the oxidation treatment [23,56,57]. Although the extension of the irradiation to 4 h caused a temporal increase in protein-like substances in the aqueous solution (Fig. 5c), all the peak intensities became weak at the end of the experiments (Fig. 5d), indicating the photocatalytic treatment of *M. aeruginosa* using the floating g-C<sub>3</sub>N<sub>4</sub> heterojunction photocatalyst is efficient in not only inactivating algal cells (Figs. 3 and 4) but also

degrading the released organic matters.

It is generally accepted that microcystin-LR is the most acute toxin from the algal COM [58]. With regard to the health risks associated with the destruction of *M. aeruginosa*, the concentrations of microcystin-LR in the aqueous solution were monitored using the liquid chromatography during the photocatalytic treatment. However, the concentrations of microcystin-LR in this study were below the detection limit. Therefore, a simulation leakage-degradation experiment was designed with the addition of 50 μg/L of microcystin-LR into the algae solution. As can be seen from Fig. S9, microcystin-LR and algae cells were simultaneously removed from the aqueous solution; e.g., at the end of the photocatalytic treatment, the removal rates of microcystin-LR and *M. aeruginosa* reached 54.7% and 74.0% respectively. This finding suggested that the presence of microcystin-LR did not cause obvious deterioration of the efficiency of the heterojunction photocatalyst in inactivation of *M. aeruginosa* though there was a competition for the active sites during dark adsorption (Fig. S9). Results of this study showed that the g-C<sub>3</sub>N<sub>4</sub> heterojunction photocatalyst is capable of degrading the intracellular microcystin-LR, if any, during the destruction of *M. aeruginosa*.

#### 3.4. Mechanisms involving the photocatalytic inactivation of *M. aeruginosa*

It has been widely reported that the photocatalytic inactivation of bacteria should be attributed to the ROSS produced by the photocatalysts [13,15,23]. In order to investigate the mechanisms involving the destruction of *M. aeruginosa* during the photocatalytic process, various active species scavengers were introduced to specify the roles of main ROSS (i.e., HO<sup>·</sup>, h<sup>+</sup>, H<sub>2</sub>O<sub>2</sub> and O<sub>2</sub><sup>−</sup>) playing in the photocatalysis; tert butyl alcohol (TBA), potassium iodide (KI), FeSO<sub>4</sub>-EDTA (Fe(II)) and benzoquinone (BQ) were used to quench HO<sup>·</sup>, h<sup>+</sup>, H<sub>2</sub>O<sub>2</sub> and O<sub>2</sub><sup>−</sup> respectively [23,59,60].

It can be seen in Fig. S10 that following the addition of BQ, Fe (II) or TBA, the efficiency of photocatalytic inactivation of *M. aeruginosa* following 6 h of irradiation were reduced to 43.6%, 44.4% or 56.4% respectively while that in the presence of KI sustained at 72.7%, indicating that O<sub>2</sub><sup>−</sup>, H<sub>2</sub>O<sub>2</sub> and HO<sup>·</sup> are likely responsible for the inactivation of cyanobacteria when the floating g-C<sub>3</sub>N<sub>4</sub> heterojunction photocatalysts used. Although the highest occupied molecular orbital (HOMO) potential of g-C<sub>3</sub>N<sub>4</sub> (i.e., 1.57 eV vs. NHE at pH of 7) is substantially lower than the standard redox potential of either HO<sup>·</sup>/OH<sup>−</sup> (+1.99 eV) or HO<sup>·</sup>/H<sub>2</sub>O (+2.37 eV) [7,20] (Scheme 1) suggesting it is

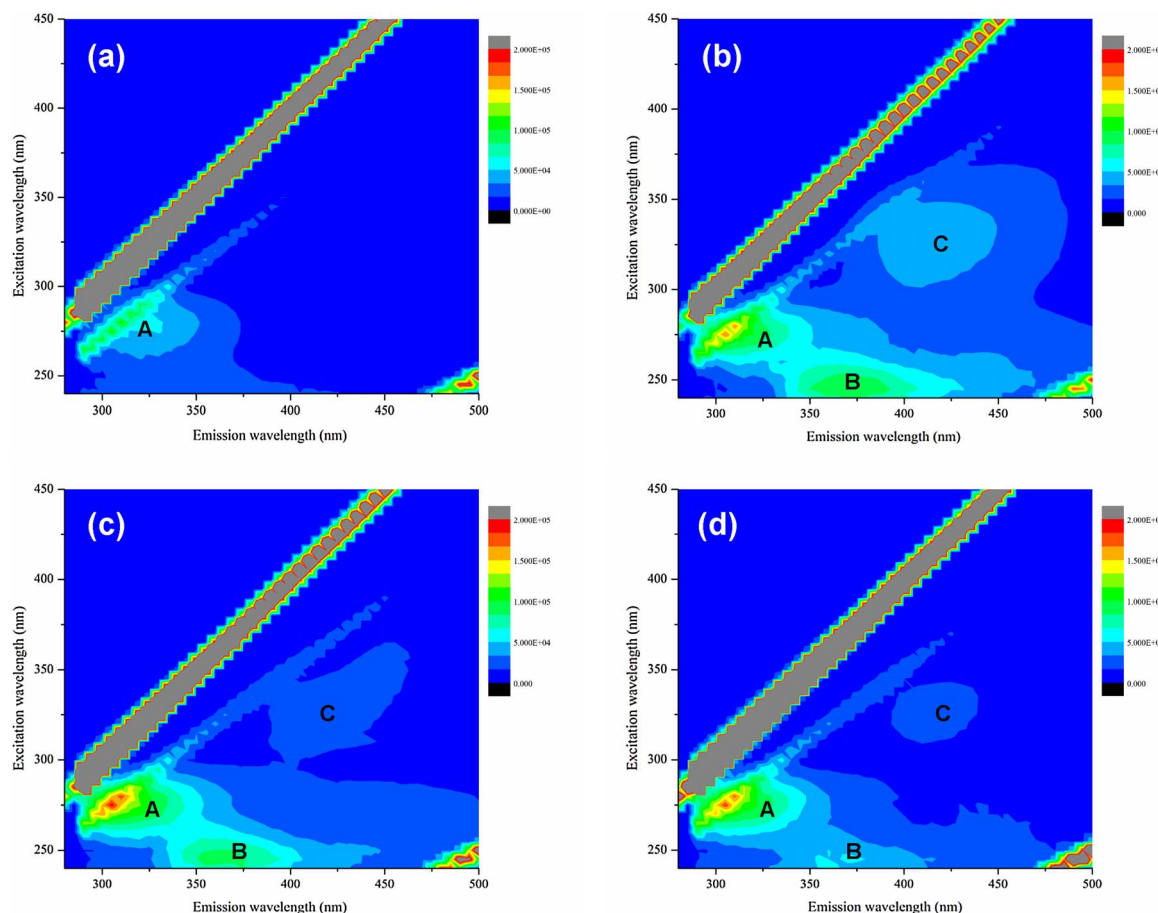
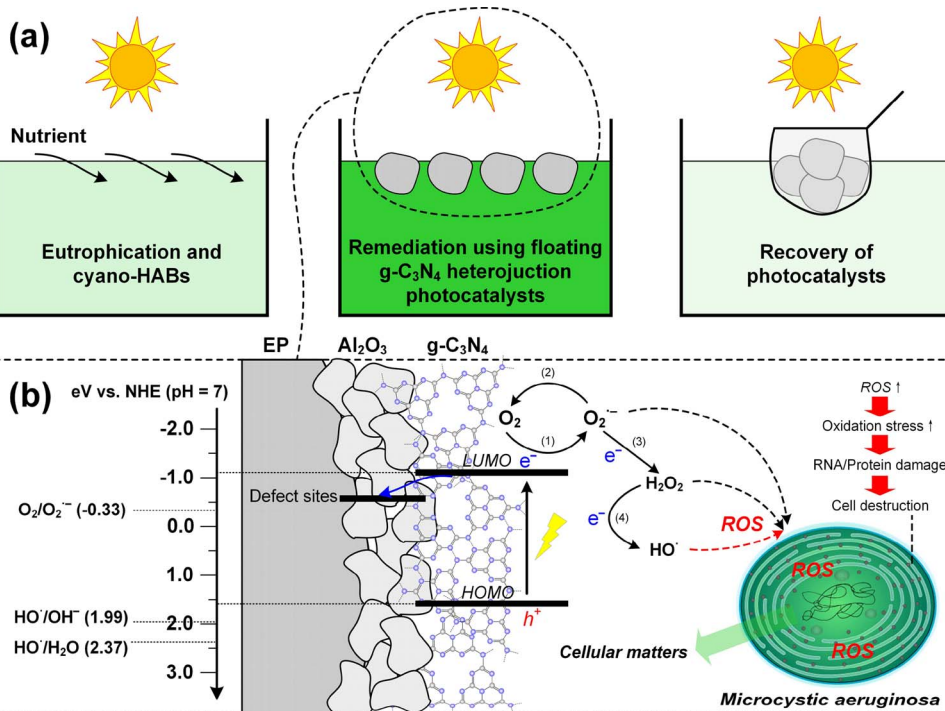
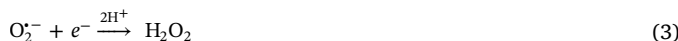


**Fig. 5.** Fluorescence EEM spectra indicating the release and degradation of cellular/extracellular organic matters during the photocatalytic treatment: (a) 0 h, (b) 2 h, (c) 4 h and (d) 6 h. Experiment conditions: CAE-2 = 0.1 g, reaction volume = 50 mL, initial cell density =  $2.7 \times 10^6$  cells/L and pH = 7.2.



**Scheme 1.** Schematic representation of the mechanisms involving the photocatalytic inactivation of *M. aeruginosa*. Numbers of the relevant reactions (Eqs. (1)–(4)) are also listed in the scheme.

unlikely that the photo-generated holes of the g-C<sub>3</sub>N<sub>4</sub> react with OH<sup>-</sup> and/or H<sub>2</sub>O to generate HO· involving the photocatalytic inactivation, the negative position of lowest unoccupied molecular orbital (LUMO) (i.e., -1.12 V) is sufficient to reduce O<sub>2</sub> to O<sub>2</sub><sup>·-</sup> (Eq. (1), E<sup>0</sup>(O<sub>2</sub>/O<sub>2</sub><sup>·-</sup>) = -0.33 eV) with the resultant O<sub>2</sub><sup>·-</sup> capable of generating HO· via a series of redox reactions (Eqs. (2)–(4)) [28,61]. To further confirm the role of H<sub>2</sub>O<sub>2</sub>, DPD/POD method was used to detect the concentration of H<sub>2</sub>O<sub>2</sub> in the photocatalytic process with the use of 2 g/L CAE-2 in deionized water [62]. However, the concentration of dissociated H<sub>2</sub>O<sub>2</sub> in the solution was not detectable after 2, 4 and 6 h visible light irradiation. It is possible to hypothesize that, during the photocatalytic process, H<sub>2</sub>O<sub>2</sub> interacts with the photoinduced electrons *in situ* once it is produced on the photocatalytic surface. As shown in Fig. S11, different concentrations of H<sub>2</sub>O<sub>2</sub> (1, 3 and 5 μM) were added to investigate the inactivation efficiency of *M. aeruginosa* by H<sub>2</sub>O<sub>2</sub>. It was found that even the addition of 5 μM H<sub>2</sub>O<sub>2</sub> did not lead to strong algal inactivation. Ding et al. [63] reported that the proliferation of *M. aeruginosa* was slightly affected even when the concentration of H<sub>2</sub>O<sub>2</sub> was up to 150 μM. Therefore, it is possible to conclude that during the photocatalytic inactivation of *M. aeruginosa*, H<sub>2</sub>O<sub>2</sub> mainly acts as the intermediate product of strong oxidizing agents (such as HO·) rather than the species directly destructing the algal cells (Eq. (4)). While it is known that h<sup>+</sup> produced from the separation of electron-hole pairs is capable of oxidizing a great number of organic compounds [28,42,43], results of this study suggested that h<sup>+</sup> is unlikely involved in the photocatalytic inactivation of *M. aeruginosa*, which is consistent with a more recent observation where Li et al. [7] reported that there was a relatively minor function for h<sup>+</sup> compared with e<sup>-</sup> that led to the production of O<sub>2</sub><sup>·-</sup> and HO· in inactivation of virus MS2. A plausible explanation is that h<sup>+</sup> generated on the surface of the heterojunction photocatalysts are readily involved in the direct inactivation of algae by contact while the presence of extracellular polymeric substances on the surface of microorganisms could induce sacrificial reactions alleviating the negative impacts on microbial metabolism in response to the direct extracellular reactions of ROSs [64]. In comparison, the free O<sub>2</sub><sup>·-</sup> and HO· in the vicinity of the catalyst surface could pass through cell membranes and subsequently increase the oxidation stress, resulting in the damage of RNA and protein and consequently the destruction of *M. aeruginosa* (Scheme 1). Further studies would be carried out to validate the relevant speculations.



Moreover, the electron transfer ability of amorphous Al<sub>2</sub>O<sub>3</sub> (e.g., the defect sites) for the electrons of g-C<sub>3</sub>N<sub>4</sub> has been reported by Li et al. [28]. In order to evaluate the role of the Al<sub>2</sub>O<sub>3</sub> layer, the photocatalytic inactivation performance of a control catalyst (CE-2) which was prepared with the same protocol of CAE-2 but without the use of Al<sub>2</sub>O<sub>3</sub> for modification was investigated. In addition, photocatalytic inactivation of *M. aeruginosa* with pure g-C<sub>3</sub>N<sub>4</sub> powder was also investigated. As shown in Fig. S12, in the absence of Al<sub>2</sub>O<sub>3</sub>, the adsorption capacity for *M. aeruginosa* was reduced with the efficiency of the photocatalytic inactivation decreased either. This finding indicated that the use of Al<sub>2</sub>O<sub>3</sub> not only enhanced the adsorption process in dark but also the separation efficiency of photo-generated electron-hole pairs of g-C<sub>3</sub>N<sub>4</sub> (Scheme 1). Since the electrons could react with the adsorbed O<sub>2</sub> to produce O<sub>2</sub><sup>·-</sup> and the following oxidants, the efficiency of CAE-2 for photocatalytic inactivation (74.4%) was much higher than that of the control catalyst (58.1%). Moreover, without the carrier of EP/Al<sub>2</sub>O<sub>3</sub>, only a small amount of algal cells (41.1%) was degraded by g-C<sub>3</sub>N<sub>4</sub> powder after 6-h irradiation (Fig. S12). These findings are, however,

not surprising because g-C<sub>3</sub>N<sub>4</sub> were suspended (and aggregated) in the bulk solution (Fig. S13) and in the solution, there was less O<sub>2</sub> for g-C<sub>3</sub>N<sub>4</sub> to produce O<sub>2</sub><sup>·-</sup> (and subsequent oxidizing agents) than near the water surface. Another problem for pure g-C<sub>3</sub>N<sub>4</sub> powder is that the visible light was also suppressed by the algal cells (Fig. S13b), which would seriously inhibit the separation of electron-hole pairs. The nano-size g-C<sub>3</sub>N<sub>4</sub> particles dispersed in the solution were difficult to be recovered which might lead to the secondary pollution to the water source. In contrast, the moderate grain size (1–3 cm) and the floating property of CAE-2 made the photocatalysts easy to be sieved by a suitable screen mesh on the water surface (Scheme 1). It can be seen from Fig. S13c that after three successive cycles, the catalysts still kept floating state following dispersed into the algal solution. As a result, CAE-2 can be used as an efficiency visible-light driven photocatalyst for the remediation of cyano-HABs in eutrophic water bodies.

#### 4. Conclusions

VLD *in situ* remediation is an attractive way against cyano-HABs in aquatic systems. However, the use of nano-size photocatalyst to enhance the contact with algae in non-stirred reservoirs would lead to the difficulty in subsequent separation and recycling of the catalysts with their residual and migration in the environment arousing serious health concerns. In this study, a novel floating g-C<sub>3</sub>N<sub>4</sub> heterojunction photocatalyst was prepared via a facile impregnation-calcination method. According to the analysis above, it can be concluded that the attack of ROSs generated under irradiation (i.e., ·OH) causes the change in membrane permeability selectivity with the cellular matters released into the solution. Meanwhile, the increase in the intracellular oxidation stress has influenced the microbial metabolism (e.g., photosynthetic activity) with cell destruction and apoptosis observed. The importance of this technology also includes the environmental significance that the floating catalyst can prevent the secondary pollution induced by the COM such as microcystin-LR. The present work thus provides a promising new dimension for fabricating photocatalysts for environmental remediation.

#### Acknowledgements

This work was financially supported by National Natural Science Foundation of China (No. 21377095). Jingke Song is supported by a scholarship from the China Scholarship Council (NO. 201706260093). Dr. Jinxing Ma acknowledges the receipt of a UNSW Vice-Chancellor's Postdoctoral Research Fellowship (RG152482).

#### Appendix A. Supplementary data

Supplementary data associated with this article can be found, in the online version, at <https://doi.org/10.1016/j.apcatb.2017.12.034>.

#### References

- [1] H. Choi, M.G. Antoniou, M. Pelaez, A.A. de la Cruz, J.A. Shoemaker, D.D. Dionysiou, Mesoporous nitrogen-Doped TiO<sub>2</sub> for the photocatalytic destruction of the cyanobacterial toxin microcystin-LR under visible light irradiation, Environ. Sci. Technol. 41 (2007) 7530–7535.
- [2] G. Zhang, Y.C. Zhang, M. Nadagouda, C. Han, K. O'Shea, S.M. El-Sheikh, A.A. Ismail, D.D. Dionysiou, Visible light-sensitized S, N and C co-doped polymorphic TiO<sub>2</sub> for photocatalytic destruction of microcystin-LR, Appl. Catal. B-Environ. 144 (2014) 614–621.
- [3] A.C.Y. Yeung, P.M. D'Agostino, A. Poljak, J. McDonald, M.W. Bligh, T.D. Waite, B.A. Neilan, Physiological and proteomic responses of continuous cultures of *Microcystis aeruginosa* PCC 7806 to changes in iron bioavailability and growth rate, Appl. Environ. Microbiol. 82 (2016) 5918–5929.
- [4] C.J. Gobler, O.M. Doherty, T.K. Hattenrath-Lehmann, A.W. Griffith, Y. Kang, R.W. Litaker, Ocean warming since 1982 has expanded the niche of toxic algal blooms in the North Atlantic and North Pacific oceans, PNAS 114 (2017) 4975–4980.
- [5] A. Zamyadi, S. Dorner, S. Sauvé, D. Ellis, A. Bolduc, C. Bastien, M. Prévost, Species-dependence of cyanobacteria removal efficiency by different drinking water

- treatment processes, *Water Res.* 47 (2013) 2689–2700.
- [6] Y. He, N.B. Sutton, H.H. Rijnaarts, A.A. Langenhoff, Degradation of pharmaceuticals in wastewater using immobilized TiO<sub>2</sub> photocatalysis under simulated solar irradiation, *Appl. Catal. B-Environ.* 182 (2016) 132–141.
- [7] Y. Li, C. Zhang, D. Shuai, S. Naraginti, D. Wang, W. Zhang, Visible-light-driven photocatalytic inactivation of MS2 by metal-free g-C<sub>3</sub>N<sub>4</sub>: virucidal performance and mechanism, *Water Res.* 106 (2016) 249–258.
- [8] M. Dlugosz, J. Waś, K. Szczubiałka, M. Nowakowska, TiO<sub>2</sub>-coated EP as a floating photocatalyst for water purification, *J. Mater. Chem. A* 2 (2014) 6931–6938.
- [9] J. Pinho, Azevedo Á, A. Brito, P. Santos, V.J. Tamagnini, V.M. Vilar, R.A. Vasconcelos, Effect of TiO<sub>2</sub> photocatalysis on the destruction of *Microcystis aeruginosa* cells and degradation of cyanotoxins microcystin-LR and cylindrospermopsin, *Chem. Eng. J.* 268 (2015) 144–152.
- [10] S. Natarajan, D.S. Lakshmi, M. Bhuvaneswari, V. Iswarya, P. Mrudula, N. Chandrasekaran, A. Mukherjee, Antifouling activities of pristine and nano-composite chitosan/TiO<sub>2</sub>/Ag films against freshwater algae, *RSC Adv.* 7 (2017) 27645–27655.
- [11] M. Pelaez, P. Falaras, V. Likodimos, A.G. Kontos, A.A. de la Cruz, K. O'shea, D.D. Dionysiou, Synthesis, structural characterization and evaluation of sol-gel-based NF-TiO<sub>2</sub> films with visible light-photoactivation for the removal of microcystin-LR, *Appl. Catal. B-Environ.* 99 (2010) 378–387.
- [12] V. Rodríguez-González, S.O. Alfaro, L. Torres-Martínez, S.-H. Cho, S.-W. Lee, Silver-TiO<sub>2</sub> nanocomposites: synthesis and harmful algae bloom UV-photo-elimination, *Appl. Catal. B-Environ.* 98 (2010) 229–234.
- [13] G. Li, X. Nie, J. Chen, Q. Jiang, T. An, P.K. Wong, H. Zhang, H. Zhao, H. Yamashita, Enhanced visible-light-driven photocatalytic inactivation of *Escherichia coli* using g-C<sub>3</sub>N<sub>4</sub>/TiO<sub>2</sub> hybrid photocatalyst synthesized using a hydrothermal-calcination approach, *Water Res.* 86 (2015) 17–24.
- [14] R. Asahi, T. Morikawa, T. Ohwaki, K. Aoki, Y. Taga, Visible-light photocatalysis in nitrogen-doped titanium oxides, *Science* 293 (2001) 269–271.
- [15] W. Wang, J.C. Yu, D. Xia, P.K. Wong, Y. Li, Graphene and g-C<sub>3</sub>N<sub>4</sub> nanosheets covaressed elemental  $\alpha$ -sulfur as a novel metal-free heterojunction photocatalyst for bacterial inactivation under visible-light, *Environ. Sci. Technol.* 47 (2013) 8724–8732.
- [16] Y. Wang, R. Shi, J. Lin, Y. Zhu, Enhancement of photocurrent and photocatalytic activity of ZnO hybridized with graphite-like C<sub>3</sub>N<sub>4</sub>, *Energy Environ. Sci.* 4 (2011) 2922–2929.
- [17] Y. Zhang, T. Mori, J. Ye, M. Antonietti, Phosphorus-Doped carbon nitride solid: enhanced electrical conductivity and photocurrent generation, *J. Am. Chem. Soc.* 132 (2010) 6294–6295.
- [18] X. Wang, K. Maeda, A. Thomas, K. Takanabe, G. Xin, J.M. Carlsson, K. Domen, M. Antonietti, A metal-free polymeric photocatalyst for hydrogen production from water under visible light, *Nat. Mater.* 8 (2009) 76–80.
- [19] S. Martha, A. Nashim, K. Parida, Facile synthesis of highly active g-C<sub>3</sub>N<sub>4</sub> for efficient hydrogen production under visible light, *J. Mater. Chem. A* 1 (2013) 7816–7824.
- [20] F. Dong, Z. Zhao, Y. Sun, Y. Zhang, S. Yan, Z. Wu, An advanced semimetal?organic bi spheres-g-C<sub>3</sub>N<sub>4</sub> nanohybrid with SPR-enhanced visible-light photocatalytic performance for NO purification, *Environ. Sci. Technol.* 49 (2015) 12432–12440.
- [21] C.A. Linkous, G.J. Carter, D.B. Locuson, A.J. Ouellette, D.K. Slattery, L.A. Smitha, Photocatalytic inhibition of algae growth using TiO<sub>2</sub>, WO<sub>3</sub>, and cocatalyst modifications, *Environ. Sci. Technol.* 34 (2000) 4754–4758.
- [22] J. Ma, Z. Wang, J. Zhang, T.D. Waite, Z. Wu, Cost-effective Chlorella biomass production from dilute wastewater using a novel photosynthetic microbial fuel cell (PMFC), *Water Res.* 108 (2017) 356–364.
- [23] X. Wang, X. Wang, J. Zhao, J. Song, J. Wang, R. Ma, J. Ma, Solar light-driven photocatalytic destruction of cyanobacteria by F-Ce-TiO<sub>2</sub>/expanded perlite floating composites, *Chem. Eng. J.* 320 (2017) 253–263.
- [24] J.G. Teeguarden, P.M. Hinderliter, G. Orr, B.D. Thrall, J.G. Pounds, Particokinetics in vitro: dosimetry considerations for in vitro nanoparticle toxicity assessments, *Toxicol. Sci.* 95 (2007) 300–312.
- [25] X. Wang, X. Wang, J. Zhao, J. Song, L. Zhou, R. Ma, J. Wang, X. Tong, Y. Chen, Efficient visible light-driven in situ photocatalytic destruction of harmful alga by worm-like N, P co-doped TiO<sub>2</sub>/expanded graphite carbon layer (NPT-EGC) floating composites, *Catal. Sci. Technol.* 7 (2017) 2335–2346.
- [26] J. Song, X. Wang, Y. Bu, X. Wang, J. Zhang, J. Huang, R. Ma, J. Zhao, Photocatalytic enhancement of floating photocatalyst: layer-by-layer hybrid carbonized chitosan and Fe-N-codoped TiO<sub>2</sub> on fly ash cenospheres, *Appl. Surf. Sci.* 391 (2016) 236–250.
- [27] F. Magalhães, F.C. Moura, R.M. Lago, TiO<sub>2</sub>/LDPE composites: a new floating photocatalyst for solar degradation of organic contaminants, *Desalination* 276 (2011) 266–271.
- [28] F.-T. Li, Y. Zhao, Q. Wang, X.-J. Wang, Y.-J. Hao, R.-H. Liu, D. Zhao, Enhanced visible-light photocatalytic activity of active Al<sub>2</sub>O<sub>3</sub>/g-C<sub>3</sub>N<sub>4</sub> heterojunctions synthesized via surface hydroxyl modification, *J. Hazard. Mater.* 283 (2015) 371–381.
- [29] C.J. Lin, Y.H. Liou, Y. Zhang, C.L. Chen, C.-L. Dong, S.Y. Chen, G.D. Stucky, Mesoporous Fe-doped TiO<sub>2</sub> sub-microspheres with enhanced photocatalytic activity under visible light illumination, *Appl. Catal. B-Environ.* 127 (2012) 175–181.
- [30] J. Xu, K.-Z. Long, Y. Wang, B. Xue, Y.-X. Li, Fast and facile preparation of metal-doped g-C<sub>3</sub>N<sub>4</sub> composites for catalytic synthesis of dimethyl carbonate, *Appl. Catal. A-Gen.* 496 (2015) 1–8.
- [31] F. Chang, J. Zhang, Y.C. Xie, J. Chen, C.L. Li, J. Wang, J.R. Luo, B.Q. Deng, X.F. Hu, Fabrication, characterization, and photocatalytic performance of exfoliated g-C<sub>3</sub>N<sub>4</sub>/TiO<sub>2</sub> hybrids, *Appl. Surf. Sci.* 311 (2014) 574–581.
- [32] P. Li, Y. Song, S. Yu, Removal of *Microcystis aeruginosa* using hydrodynamic cavitation: performance and mechanisms, *Water Res.* 62 (2014) 241–248.
- [33] X.Q. Lyu, Y.L. Zhang, W.H. You, Growth and physiological responses of Eichhornia crassipes to clonal integration under experimental defoliation, *Aquat. Ecol.* 50 (2016) 153–162.
- [34] Z. Wang, Z. Wu, S. Tang, Characterization of dissolved organic matter in a submerged membrane bioreactor by using three-dimensional excitation and emission matrix fluorescence spectroscopy, *Water Res.* 43 (2009) 1533–1540.
- [35] F. Yanfen, H. Yingping, Y. Jing, W. Pan, C. Genwei, Unique ability of BiOBr to decarboxylate D-Glu and D-MeAsp in the photocatalytic degradation of microcystin-LR in water, *Environ. Sci. Technol.* 45 (2011) 1593–1600.
- [36] H. Jiao, X. Zhao, C. Lv, Y. Wang, D. Yang, Z. Li, X. Yao, Nb<sub>2</sub>O<sub>5</sub>- $\gamma$ -Al<sub>2</sub>O<sub>3</sub> nanofibers as heterogeneous catalysts for efficient conversion of glucose to 5-hydroxymethylfurfural, *Sci. Rep. U.K.* 6 (2016) 34068.
- [37] Q. Li, Y. Zhang, Z. Cao, W. Gao, L. Cui, Crystallization behavior of zeolite beta from acid-leached metakaolin, *Petrol Sci.* 7 (2010) 541–546.
- [38] J.X. Sun, Y.P. Yuan, L.G. Qiu, X. Jiang, A.J. Xie, Y.H. Shen, J.F. Zhu, Fabrication of composite photocatalyst g-C<sub>3</sub>N<sub>4</sub>/ZnO and enhancement of photocatalytic activity under visible light, *Dalton Trans.* 41 (2012) 6756–6763.
- [39] T. Li, L. Zhao, Y. He, J. Cai, M. Luo, J. Lin, Synthesis of g-C<sub>3</sub>N<sub>4</sub>/SmVO<sub>4</sub> composite photocatalyst with improved visible light photocatalytic activities in RhB degradation, *Appl. Catal. B-Environ.* 129 (2013) 255–263.
- [40] M. Donohue, G. Aranovich, Classification of Gibbs adsorption isotherms, *Adv. Colloid Interface Sci.* 76 (1998) 137–152.
- [41] S.H. Chai, H.P. Wang, Y. Liang, B.X. Xu, Sustainable production of acrolein: gas-phase dehydration of glycerol over Nb<sub>2</sub>O<sub>5</sub> catalyst, *J. Catal.* 250 (2007) 342–349.
- [42] Z. Lu, L. Zeng, W.L. Song, Z.Y. Qin, D.W. Zeng, C.S. Xie, In situ synthesis of C-TiO<sub>2</sub>/g-C<sub>3</sub>N<sub>4</sub> heterojunction nanocomposite as highly visible light active photocatalyst originated from effective interfacial charge transfer, *Appl. Catal. B-Environ.* 202 (2017) 489–499.
- [43] Y.H. Li, K.L. Lv, W.K. Ho, F. Dong, X.F. Wu, Y. Xia, Hybridization of rutile TiO<sub>2</sub> (rTiO<sub>2</sub>) with g-C<sub>3</sub>N<sub>4</sub> quantum dots (CN QDs): An efficient visible-light-driven Z-scheme hybridized photocatalyst, *Appl. Catal. B-Environ.* 202 (2017) 611–619.
- [44] J. Li, M. Zhang, Q.Y. Li, J.J. Yang, Enhanced visible light activity on direct contact Z-scheme g-C<sub>3</sub>N<sub>4</sub>/TiO<sub>2</sub> photocatalyst, *Appl. Surf. Sci.* 391 (2017) 184–193.
- [45] J.C. Sanchez-Lopez, C. Donnet, F. Lefebvre, C. Fernandez-Ramos, A. Fernandez, Bonding structure in amorphous carbon nitride: a spectroscopic and nuclear magnetic resonance study, *J. Appl. Phys.* 90 (2001) 675–681.
- [46] S. Stankovich, R.D. Piner, X.Q. Chen, N.Q. Wu, S.T. Nguyen, R.S. Ruoff, Stable aqueous dispersions of graphitic nanoplatelets via the reduction of exfoliated graphite oxide in the presence of poly(sodium 4-styrenesulfonate), *J. Mater. Chem.* 16 (2006) 155–158.
- [47] J. Fu, F. Pi, Q. Dong, H. Duan, A cost-effective solid-state approach to synthesize g-C<sub>3</sub>N<sub>4</sub> coated TiO<sub>2</sub> nanocomposites with enhanced visible light photocatalytic activity, *Int. J. Photoenergy* 2013 (2013).
- [48] S. Gredelj, A.R. Gerson, S. Kumar, N.S. McIntyre, Plasma nitriding and in situ characterisation of aluminium, *Appl. Surf. Sci.* 199 (2002) 234–247.
- [49] Z.C. Wang, M. Zuo, Y.C. Wang, Y.D. Liu, D.H. Li, Dynamics of chlorophyll fluorescence and eco-Morphological properties of microcysts bloom in meiliang bay of lake taihu, China, *Fresenius Environ. Bull.* 20 (2011) 2295–2305.
- [50] E.M. Tytler, G.C. Whitelam, M.F. Hipkins, G.A. Codd, Photoinactivation of photosystem II during photoinhibition in the cyanobacterium *Microcystis aeruginosa*, *Planta* 160 (1984) 229–234.
- [51] X. Wang, X. Wang, J. Zhao, J. Song, L. Zhou, J. Wang, X. Tong, Y. Chen, An alternative to in situ photocatalytic degradation of microcystin-LR by worm-like N, P co-doped TiO<sub>2</sub>/expanded graphite by carbon layer (NPT-EGC) floating composites, *Appl. Catal. B-Environ.* 206 (2017) 479–489.
- [52] J. Niu, Y. Li, W. Wang, Light-source-dependent role of nitrate and humic acid in tetracycline photolysis: kinetics and mechanism, *Chemosphere* 92 (2013) 1423–1429.
- [53] S. Zhou, Y. Shao, N. Gao, S. Zhu, L. Li, J. Deng, M. Zhu, Removal of *Microcystis aeruginosa* by potassium ferrate (VI): Impacts on cells integrity, intracellular organic matter release and disinfection by-products formation, *Chem. Eng. J.* 251 (2014) 304–309.
- [54] F.G. Karimova, E.E. Kortchouganova, I.A. Tarchevsky, M.R. Iagoucheva, The oppositely directed Ca<sup>2+</sup> and Na<sup>+</sup> transmembrane transport in algal cells, *Protoplasma* 213 (2000) 93–98.
- [55] W. Chen, P. Westerhoff, J.A. Leenheer, K. Booksh, Fluorescence excitation-Emission matrix regional integration to quantify spectra for dissolved organic matter, *Environ. Sci. Technol.* 37 (2003) 5701–5710.
- [56] L. Li, C. Shao, T.-F. Lin, J. Shen, S. Yu, R. Shang, D. Yin, K. Zhang, N. Gao, Kinetics of cell inactivation, toxin release, and degradation during permanganation of microcysts aeruginosa, *Environ. Sci. Technol.* 48 (2014) 2885–2892.
- [57] F. Qu, H. Liang, J. He, J. Ma, Z. Wang, H. Yu, G. Li, Characterization of dissolved extracellular organic matter (dEOM) and bound extracellular organic matter (bEOM) of *Microcystis aeruginosa* and their impacts on UF membrane fouling, *Water Res.* 46 (2012) 2881–2890.
- [58] L. Li, N. Gao, Y. Deng, J. Yao, K. Zhang, Characterization of intracellular & extracellular algae organic matters (AOM) of *Microcystis aeruginosa* and formation of AOM-associated disinfection byproducts and odor & taste compounds, *Water Res.* 46 (2012) 1233–1240.
- [59] J. Song, X. Wang, J. Huang, J. Ma, X. Wang, H. Wang, R. Ma, P. Xia, J. Zhao, High performance of N-doped TiO<sub>2</sub>-magnetic activated carbon composites under visible light illumination: synthesis and application in three-dimensional photoelectrochemical process, *Electrochim. Acta* 222 (2016) 1–11.
- [60] W. Wang, L. Zhang, T. An, G. Li, H.-Y. Yip, P.-K. Wong, Comparative study of visible-light-driven photocatalytic mechanisms of dye decolorization and bacterial disinfection by B?Ni-codoped TiO<sub>2</sub> microspheres: the role of different reactive species, *Appl. Catal. B: Environ.* 108–109 (2011) 108–116.

- [61] J. Ma, D. He, R.N. Collins, C. He, T.D. Waite, The tortoise versus the hare-Possible advantages of microparticulate zerovalent iron (mZVI) over nanoparticulate zerovalent iron (nZVI) in aerobic degradation of contaminants, *Water Res.* 105 (2016) 331–340.
- [62] H. Bader, V. Sturzenegger, J. Hoigne, Photometric method for the determination of low concentrations of hydrogen peroxide by the peroxidase catalyzed oxidation of N, N-diethyl-p-phenylenediamine (DPD), *Water Res.* 22 (1988) 1109–1115.
- [63] Y. Ding, N. Gan, J. Li, B. Sedmak, L. Song, Hydrogen peroxide induces apoptotic-like cell death in *Microcystis aeruginosa* (Chroococcales, Cyanobacteria) in a dose-dependent manner, *Phycologia* 51 (2012) 567–575.
- [64] X. Han, Z. Wang, M. Chen, X. Zhang, C.Y. Tang, Z. Wu, Acute responses of microorganisms from membrane bioreactors in the presence of NaOCl: protective mechanisms of extracellular polymeric substances, *Environ. Sci. Technol.* 51 (2017) 3233–3241.